

Cite this article as: Ma Kai, Feng Li. Microstructure and Properties of FeCrMnAlCu HEA Coatings Synthesized by Induction Remelting and Laser Remelting[J]. Rare Metal Materials and Engineering, 2023, 52(01): 111-118.

ARTICLE

Microstructure and Properties of FeCrMnAlCu HEA Coatings Synthesized by Induction Remelting and Laser Remelting

Ma Kai¹, Feng Li^{1,2}

¹ School of Materials Science and Technology, Lanzhou University of Technology, Lanzhou 730050, China; ² State Key Laboratory of Advanced Processing and Recycling of Nonferrous Metals, Lanzhou University of Technology, Lanzhou 730050, China

Abstract: FeCrMnAlCu high-entropy alloy (HEA) coatings were prepared on the surface of 45# steel by cold spraying-assisted induction remelting and cold spraying-assisted laser remelting. The phase composition, microstructure, microhardness, and wear resistance of the HEA coatings were characterized, and the effects of the two processes on the wear resistance of HEA coatings were studied. Results show that the FeCrMnAlCu HEA coatings synthesized by these two methods are composed of body-centered cubic (bcc) and face-centered cubic (fcc) phases. The coating microstructure is dense and the elements are evenly distributed. The microstructures of coatings consist of dendrite+interdendrite structures, and the dendrite region is mainly enriched with Mn, Cr, and Fe elements, while the interdendrite region is rich in Cu. In addition, the Al element is evenly distributed between the dendrite and interdendrite. The lattice strain of bcc phase in FeCrMnAlCu HEA coating synthesized by cold spraying-assisted induction remelting is greater than that by cold spraying-assisted laser remelting. The microhardness of the FeCrMnAlCu HEA coating synthesized by cold spraying-assisted induction remelting is 1.2 times higher than that by cold spraying-assisted laser remelting and 3.5 times higher than that of the 45# steel matrix. The friction process of FeCrMnAlCu HEA coating is mainly the abrasive wear. The FeCrMnAlCu HEA coating synthesized by cold spraying-assisted induction remelting has good wear resistance, and its wear rate is 29% lower than that by cold spraying-assisted laser remelting.

Key words: induction remelting; laser remelting; HEA coating; lattice strain

Since Yeh^[1] and Cantor^[2] et al proposed the multi-principal component high-entropy alloy (HEA), which typically contains five or more elements with approximately equal atomic ratios (5at%–35at% for the main elements and <5at% for the secondary elements), it has been widely researched and used^[3–7]. Various main elements can lead to the high entropy effect of HEAs in thermodynamics, such as the lattice distortion effect in structure, the hysteretic diffusion effect in dynamics, the cocktail effect in properties, and structural stability. These effects are beneficial to improve the mechanical properties of HEAs, such as high strength, good corrosion resistance, and excellent wear resistance^[8–10]. HEAs are commonly composed of Ni, Co, Fe, Cr, Ti, Al, Cu, W, and Zr elements, such as NiCoCrFeAlCu, AlCrFeCuCo,

AlTiCrFeCoNi, CuZrAlTiNi, and CrMoNbTiW HEAs^[11–15]. Among them, the treatment cost of Ni, Co, Ti, and W accounts for a large part.

Mn is an inexpensive metallic element with abundant sources, thereby attracting much attention as an alloying element^[16]. Ye et al^[17] prepared CrMnFeCoNi HEA coatings by laser cladding, which have the single face-centered cubic (fcc) phase structure. The microstructure of HEA coating consists of columnar dendrite, and the CrMnFeCoNi HEA coating shows good corrosion resistance in H₂SO₄ solution. Wong et al^[18] prepared Al_{0.3}CoCrFeNiMn_x HEA coatings by induction melting and air casting and found that the microstructures of these HEA coatings are all simple fcc structures. With increasing the Mn content, the lattice parameter of the

Received date: March 31, 2022

Foundation item: National Key R&D Program of China (2016YFE0111400); National Nature Science Foundation China (52075234); Young Doctor Fund Project of Gansu Province (2021QB-043)

Corresponding author: Feng Li, Ph. D., Professor, School of Materials Science and Engineering, Lanzhou University of Technology, Lanzhou 730050, P. R. China, E-mail: fenglills@lut.edu

Copyright © 2023, Northwest Institute for Nonferrous Metal Research. Published by Science Press. All rights reserved.

$Al_{0.3}CoCrFeNiMn_x$ HEA coating is increased from 0.3591 nm to 0.3611 nm, and the coating hardness is increased from 1382 MPa to 1529 MPa. Liao et al^[19] prepared the CoCrFeNiMn HEA coating on 316L stainless steel substrate by explosive spraying. The coating microstructure is dense of simple fcc phases and the coating contains a small amount of flocculated metal oxide at nanoscale. It is found that the microhardness of the explosive-sprayed CoCrFeNiMn coating is significantly higher than that of the HEA coating prepared by direct casting and spark plasma sintering due to the effect of grain refinement strengthening. Yin et al^[20] prepared the FeCoNiCrMn HEA coating on 45# steel substrate by cold spraying. The coating does not undergo phase transformation, resulting in excellent mechanical properties.

In this research, the Mn element was used to replace Ni, Co, and other elements to reduce the production cost and to improve the friction properties of the coating. The FeCrMnAlCu HEA coatings with a thickness of 400 μm were prepared by cold spraying-assisted induction remelting and cold spraying-assisted laser remelting^[21-22]. The effects of different preparation methods of FeCrMnAlCu HEA coating on the wear resistance of coating were investigated.

1 Experiment

The raw materials used in this research were commercial Fe, Cr, Mn, Al, and Cu (purity \geq 99.5%) powders. The metal powders were mechanically mixed for 4 h and used as cold spraying prefabrication material. The morphology of the prefabricated cold-sprayed mixture powders is shown in Fig. 1a, where Cu and Fe are dendritic electrolytic powders, Al and Mn are spherically-atomized powders, and Cr is broken powder with an irregular morphology. Different metal powders have different deposition ratios under the same cold spraying process. In this experiment, the deposition ratio of different metal elements is as following: Fe:Cr:Mn:Al:Cu=3:6:2:1:1.4 (at%). The base material was 45# steel matrix. Before spraying, the acetone was used to ultrasonically remove the oil and other impurities on the steel surface, and the sand blasting was conducted to roughen the substrate surface. Table 1 shows the composition of cold-sprayed HEA coating.

Low pressure cold spraying equipment (GDU-3-15, Belarus) was used to prepare the coatings on 45# steel matrix. Table 2 shows the process parameters of cold spraying treatment. The heating power of induction remelting was 1.5–2.2 kW, and the heating duration was 15–20 s. HEA coatings were synthesized by induction remelting of mixed coatings prepared by cold spraying. Table 3 shows the composition of HEA coating after induction remelting.

Yls-400 fiber laser (IPG Company, Germany) was adopted for laser remelting. The process parameters of the laser remelting treatment are shown in Table 4. Table 5 shows the composition of HEA coating after laser remelting.

Quanta FEG450 field emission scanning electron microscope (SEM) and energy dispersive spectrometer (EDS) were used to analyze the surface morphology and composition of prefabricated mixed coating and HEA coating. Transmission

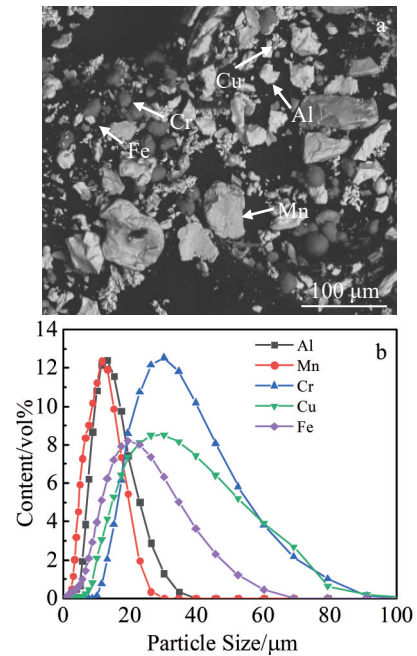


Fig.1 Morphology (a) and particle size distribution (b) of prefabricated cold-sprayed mixture powder

Table 1 Composition of cold-sprayed FeCrMnAlCu coating (wt%)

Fe	Cr	Mn	Al	Cu
22.38	44.78	14.00	7.46	10.44

Table 2 Process parameters of cold spraying treatment

Parameter	Value
Working gas	Compressed air
Temperature/ $^{\circ}\text{C}$	500
Pressure/MPa	0.7–0.8
Spraying distance/mm	10–20
Spraying speed/ $\text{m}\cdot\text{s}^{-1}$	0.4–0.6

Table 3 Composition of cold-sprayed FeCrMnAlCu coating after induction remelting (wt%)

Fe	Cr	Mn	Al	Cu
29.3	17.7	15.5	18.3	15.5

Table 4 Process parameters of laser remelting treatment

Parameter	Value
Power/W	2200
Scanning speed/ $\text{mm}\cdot\text{s}^{-1}$	500
Shielding gas/ $\text{L}\cdot\text{min}^{-1}$	0.7–0.8
Light spot diameter/mm	10–20
Overlapping ratio/%	0.4–0.6

electron microscope (TEM) was used to analyze the microstructure of HEA coating. An HV-1000 type

Table 5 Composition of cold-sprayed FeCrMnAlCu coating after laser remelting (wt%)

Fe	Cr	Mn	Al	Cu
30.3	17.1	14.6	17.4	20.6

microhardness tester was used to measure the Vickers hardness of the specimen at 15 points under the load of 0.5 N. CSM friction and wear tester was used to test the friction performance of the coating under dry friction conditions. The size of the friction specimen was 20 mm×20 mm×5 mm, the grinding ball was composed of alumina ($\Phi 6$ mm), the test load was 7.5 N, and the test duration was 20 min. Each experiment was repeated three times, and the average value was used for analysis. In addition, the friction length was 3 mm and the sliding frequency f was 3 Hz. The wear rate of the coating can be calculated by Eq.(1)^[23], as follows:

$$\sigma = \frac{v}{\sum W} = \frac{AL}{2FTfL} \quad (1)$$

where σ is the wear rate ($\text{mm}^3 \cdot \text{N}^{-1} \cdot \text{m}^{-1}$), V represents the volume of friction slid mark, W is the accumulated frictional work (N·m), A is the cross-sectional area of wear, L is the abrasion mark length (mm), F is the applied load force (N), and f is the sliding frequency (Hz).

2 Results and Discussion

2.1 Microstructure and phase composition of prefabricated cold-sprayed mixture coating

Fig. 2 shows SEM cross-section morphology and XRD pattern of the cold-sprayed FeCrMnAlCu mixture coating. It can be seen from Fig. 2a that the cold-sprayed coating has dense structure and small dispersed pores. According to

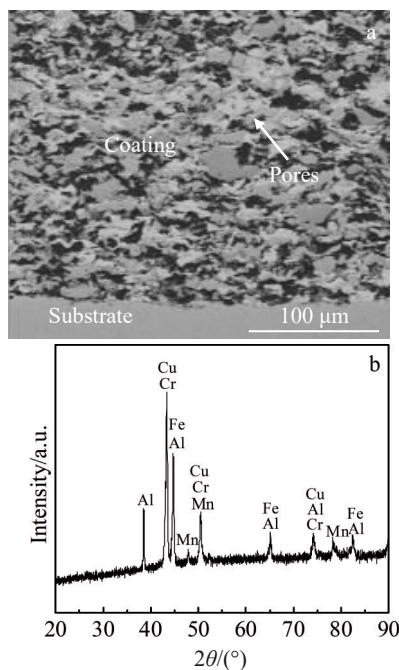


Fig.2 SEM cross-section morphology (a) and XRD pattern (b) of cold-sprayed FeCrMnAlCu mixture coating

Fig.2b, the powder particles in the coating exist in the metallic form.

2.2 Phase composition of FeCrMnAlCu HEA coating by induction remelting and laser remelting

Fig. 3 shows XRD patterns of the FeCrMnAlCu HEA coatings prepared by cold spraying-assisted induction remelting and cold spraying-assisted laser remelting. It can be seen that the FeCrMnAlCu HEA coating is composed of simple body-centered cubic (bcc) and fcc phases.

The entropy of HEAs can be determined by mixing entropy ΔS_{mix} . Ω is a parameter of mixing entropy and δ is the atomic size difference. The relationship among these parameters are as follows^[24-26]:

$$\Delta S_{\text{mix}} = -R \sum_{i=1}^n c_i \ln c_i \quad (2)$$

where c_i is the content of i component (at%); R is the gas constant ($8.314 \text{ J} \cdot \text{mol}^{-1} \cdot \text{K}^{-1}$); n is the total number of components. Therefore, Eq.(3) can be obtained, as follows:

$$\Omega = \frac{T_m \Delta S_{\text{mix}}}{|\Delta H_{\text{mix}}|} \quad (3)$$

where T_m is the phase transition temperature and H_{mix} is the enthalpy of mixture. In addition, δ can be calculated by Eq.(4), as follows:

$$\delta = \sqrt{\sum_{i=1}^n x_i \left(1 - \frac{r_i}{\bar{r}}\right)^2} \quad (4)$$

where r_i is the atomic radius of i component; \bar{r} is the average atomic radius with $\bar{r} = \sum_{i=1}^n c_i r_i$.

When the conditions of $\Delta S_{\text{mix}} \geq 1.61R$, $\Omega \geq 6.6$, and $\delta \leq 6.6$ are satisfied in the HEA system, HEA can easily form a stable solid solution structure. Table 6 shows the parameters of the

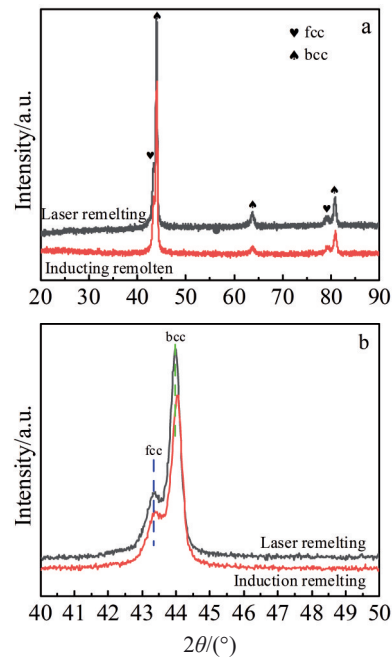


Fig.3 XRD patterns of $2\theta=20^\circ-90^\circ$ (a) and $2\theta=40^\circ-50^\circ$ (b) for FeCrMnAlCu HEA coatings prepared by cold spraying-assisted induction remelting and laser remelting

Table 6 Parameters of FeCrMnAlCu HEA coating with stable solid solution structure

Parameter	Value
Enthalpy of mixture, $H_{\text{mix}}/\text{kJ}\cdot\text{mol}^{-1}$	-1.76
Entropy of mixture, S_{mix}	1.61R
Parameter, Ω	9.6
Atomic size difference, $\delta/\%$	4.89

FeCrMnAlCu HEA coating with a stable solid solution structure. Based on the calculation results and XRD analysis results from Fig.3a, it can be concluded that the FeCrMnAlCu HEA coating is composed of simple bcc and fcc phases.

According to Bragg equation, the lattice constants of the bcc phase in HEA coating after cold spraying-assisted induction remelting and laser remelting are 0.284 67 and 0.285 16 nm, respectively. The peak shift of the fcc phase can barely be noticed. According to Table 3 and Table 5, this phenomenon is mainly due to the high content of Fe in FeCrMnAlCu HEA synthesized by cold spraying-assisted laser remelting.

2.3 Microstructure of FeCrMnAlCu HEA coating by cold spraying-assisted induction remelting and laser remelting

Fig. 4 shows SEM cross-section and surface morphologies of FeCrMnAlCu HEA coating prepared by cold spraying-assisted induction remelting and EDS analysis results of dendrite and interdendrite regions. As shown in Fig. 4a, the coating is well combined with the matrix. According to Fig.4b–4d, the coating microstructure is mainly composed of den-

drite and a small amount of interdendrite. The dendrite size is 0.86 μm , and the proportion of dendrite structure is 87%. The dendrite region is mainly rich in Mn, Cr, and Fe, while the interdendrite region is rich in Cu element. In addition, Al element is evenly distributed between the dendrite and interdendrite regions.

Fig. 5 shows SEM cross-section and surface morphologies of FeCrMnAlCu HEA coating prepared by cold spraying-assisted laser remelting and EDS analysis results of dendrite and interdendrite regions. According to Fig.5a, the coating is well combined with the substrate. The coating microstructure is also composed of dendrite and interdendrite. The dendrite size is 0.72 μm , and the proportion of dendrite structure is 74%. The laser remelting process exhibits concentrated energy and high temperature, resulting in thick heat-affected zone and Fe diffusion into the coating. Therefore, more Fe exists between the dendrite and interdendrite regions. The dendrite is mainly rich in Mn, Cr, and Fe, while the interdendrite region is rich in Cu element. In addition, Al element is evenly distributed between the dendrite and interdendrite regions.

Fig. 6 shows TEM bright field images of FeCrMnAlCu HEA coatings prepared by cold spraying-assisted induction remelting and laser remelting and selected area electron diffraction (SAED) patterns of bcc and fcc phases in FeCrMnAlCu HEA coating prepared by cold spraying-assisted induction remelting. It can be seen that the HEA coating is composed of dendritic bcc phase and interdendritic fcc phase. According to Fig. 6, the microstructure of HEA coating synthesized by induction remelting and laser remelting is both composed of dendrite and interdendrite.

The excellent performance of HEA coating is primarily

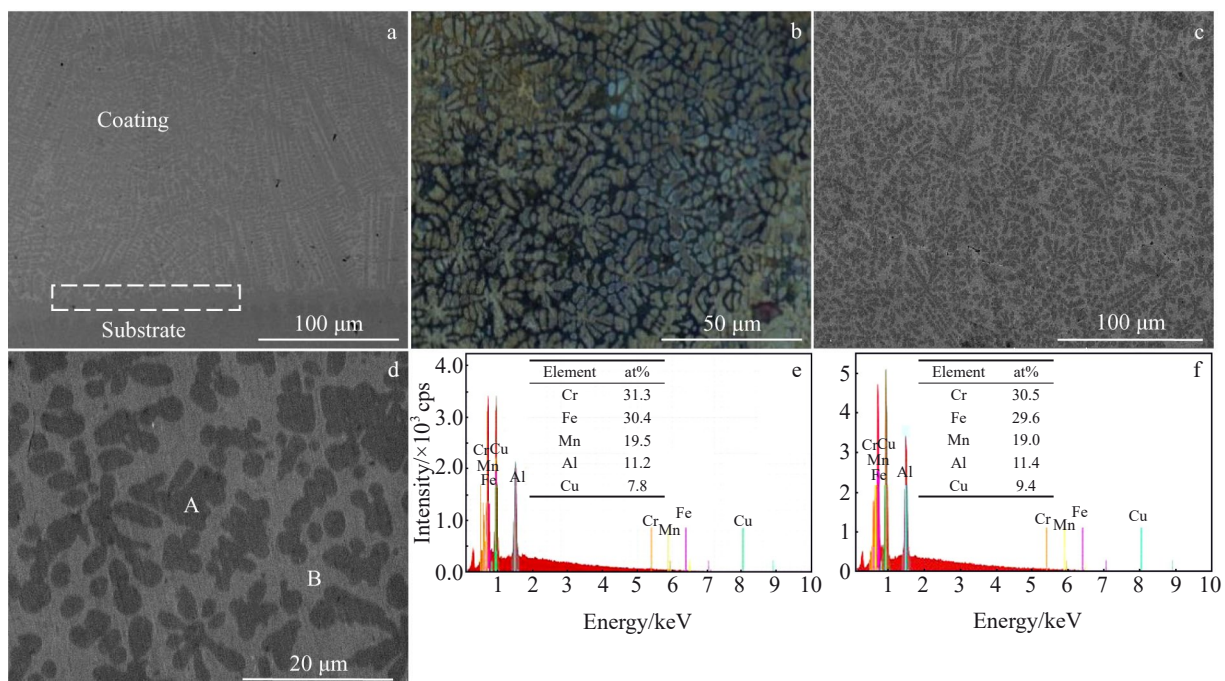


Fig.4 SEM cross-section (a) and surface (b–d) morphologies of FeCrMnAlCu HEA coating prepared by cold spraying-assisted induction remelting; EDS analysis results of dendrite-point A (e) and interdendrite-point B (f) in Fig.4d

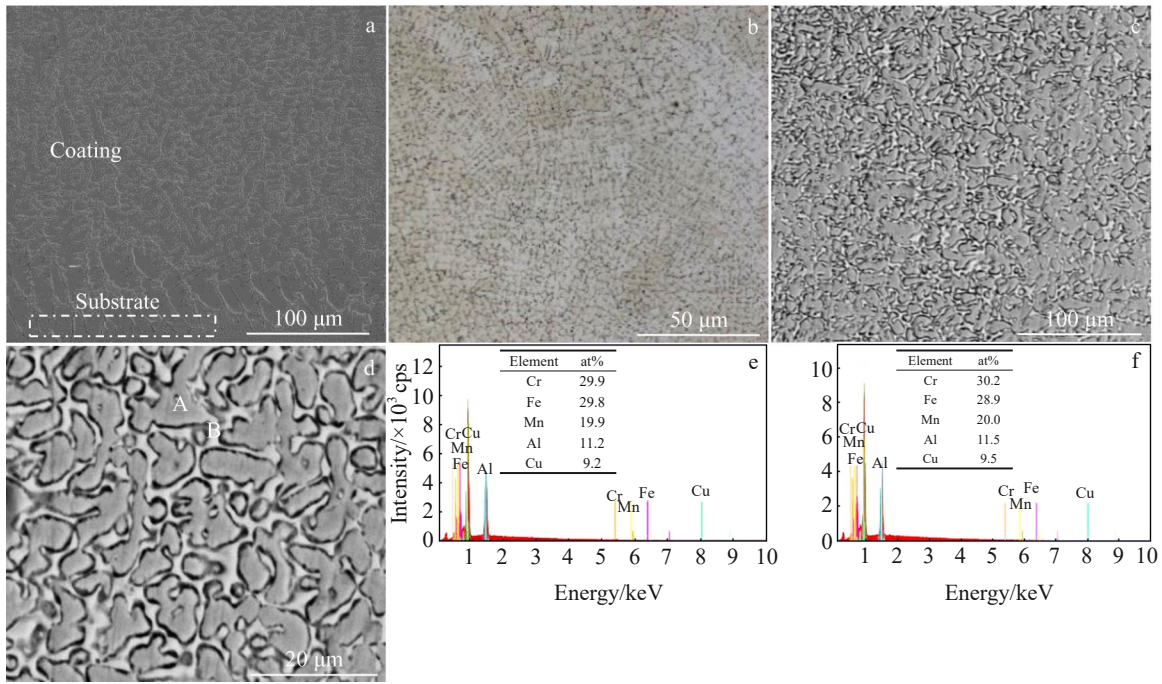


Fig.5 SEM cross-section (a) and surface (b–d) morphologies of FeCrMnAlCu HEA coating prepared by cold spraying-assisted laser remelting; EDS analysis results of dendrite-point A (e) and interdendrite-point B (f) in Fig.5d

derived from the lattice distortion effect of HEA, which can be expressed by lattice strain $\epsilon^{[27]}$, as follows:

$$\epsilon = \Delta a/a_0 \tag{5}$$

$$\Delta a = |a - a_0| \tag{6}$$

where a and a_0 are the lattice constants of the actual and ideal lattices, respectively. The lattice strain ϵ of fcc and bcc phases in FeCrMnAlCu HEAs synthesized by cold spraying-assisted induction remelting and laser remelting is decreased with increasing the atomic size. Therefore, based on the abovementioned results, in FeCrMnAlCu HEAs synthesized by cold spraying-assisted induction remelting, the lattice strain of bcc phase is 0.84%, the lattice strain of fcc phase is 3.85%, and the atomic size difference is 9.36%. In FeCrMnAlCu HEAs synthesized by cold spraying-assisted laser remelting, the lattice strain of bcc phase is 0.75%, the lattice strain of fcc phase is 3.73%, and the atomic size difference is 9.14%. In conclusion, the more obvious the deformation, the more intense the lattice distortion of the alloy.

2.4 Microhardness and friction properties of FeCrMnAlCu HEA coatings prepared by cold spraying-assisted induction remelting and laser remelting

Fig. 7a shows the microhardness of FeCrMnAlCu HEA coatings synthesized by cold spraying-assisted induction remelting and laser remelting. The microhardness HV of FeCrMnAlCu HEA coatings synthesized by cold spraying-assisted induction remelting and laser remelting is 5742.8 and 4739.3 MPa, respectively. The microhardness of 45# steel matrix is 1668.0 MPa. The microhardness of the FeCrMnAlCu HEA coating synthesized by cold spraying-assisted induction remelting is 5742.8 MPa, which is 1.2 times

higher than that synthesized by cold spraying-assisted laser remelting, and 3.5 times higher than that of 45# steel matrix. Fig. 7b shows the friction coefficient of the 45# steel matrix and FeCrMnAlCu HEA coatings. The friction coefficient of 45# steel matrix is 0.69, and that of the FeCrMnAlCu HEA coatings synthesized by cold spraying-assisted induction remelting and laser-remelting is 0.35 and 0.48, respectively. Under the same friction conditions, the higher the microhardness/strength, the stronger the deformation resistance, but the worse the wear resistance^[28]. The high microhardness of the FeCrMnAlCu HEA coating synthesized by cold spraying-assisted induction remelting is primarily due to the following aspects. (1) The lattice strain of the bcc phase and fcc phase in the FeCrMnAlCu HEA coating synthesized by cold spraying-assisted induction remelting is larger than that prepared by cold spraying-assisted laser remelting. Therefore, the solid solution strengthening is sufficient and the microhardness of is high. The laser remelting leads to the high diffusion of Fe element into the HEA coating, thereby decreasing the lattice strain. (2) The proportion of dendritic bcc structure of high microhardness in the FeCrMnAlCu HEA coating synthesized by cold spraying-assisted induction remelting is larger than that synthesized by cold spraying-assisted laser remelting. Therefore, the HEA coating prepared by cold spraying-assisted induction remelting exhibits higher microhardness due to the large amount of bcc phase.

Fig. 8 shows the friction and wear morphologies of the FeCrMnAlCu HEA coatings prepared by cold spraying-assisted induction remelting and laser remelting. The wear rates of the FeCrMnAlCu HEA coatings prepared by cold spraying-assisted induction remelting and laser remelting are

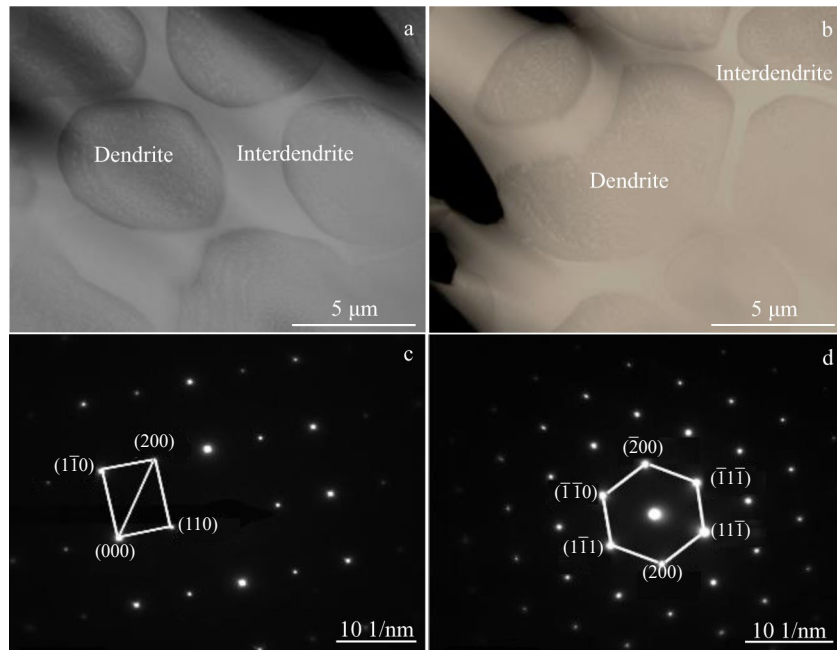


Fig.6 TEM bright field images of FeCrMnAlCu HEA coatings prepared by cold spraying-assisted induction remelting (a) and laser remelting (b); SAED patterns of bcc (c) and fcc (d) phases in FeCrMnAlCu HEA coating prepared by cold spraying-assisted induction remelting

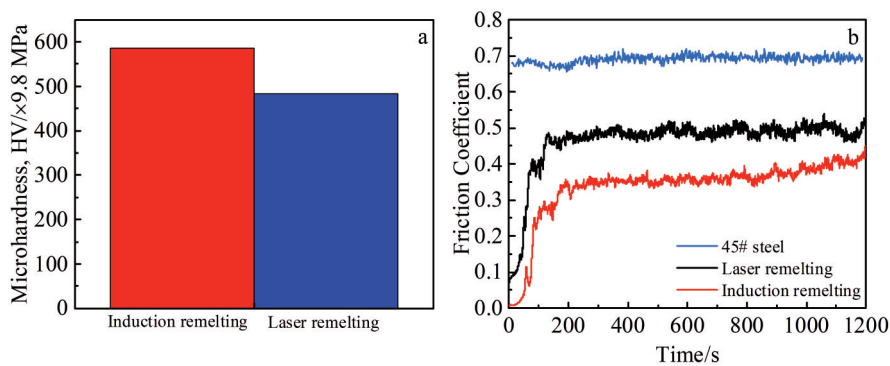


Fig.7 Microhardness of different FeCrMnAlCu HEA coatings (a); friction coefficient of 45# steel and different FeCrMnAlCu HEA coatings (b)

2.95×10^{-5} and $4.14 \times 10^{-5} \text{ mm}^3 \cdot \text{N}^{-1} \cdot \text{m}^{-1}$, respectively. Compared with that prepared by cold spraying-assisted laser remelting, the wear rate of HEA coating prepared by cold spraying-assisted induction remelting reduces by 29%. According to Ref.[29], it is known that the wear resistance of the coating is positively correlated with the coating hardness. The greater the coating hardness, the better the wear resistance and the lower the wear rate. The FeCrMnAlCu HEA coating synthesized by cold spraying-assisted induction remelting has relatively higher microhardness, which leads to the lower wear rate and better wear resistance.

Fig. 9 shows the morphologies of wear surface and wear debris of FeCrMnAlCu HEA coatings. It can be seen that the FeCrMnAlCu HEA coating synthesized by cold spraying-assisted induction remelting has a smooth surface with a few shallow furrows. In addition, there is a little delamination in the coating, which significantly reduces the adhesive wear, thereby resulting in the low friction coefficient. According to

Fig.9d, the FeCrMnAlCu HEA coating synthesized by cold spraying-assisted laser remelting has a rough surface. A large number of deep furrows and flaky layers appear on the coating surface. The morphology of the worn surface shows that the wear mechanism of the FeCrMnAlCu HEA coating synthesized by cold spraying-assisted induction remelting and laser remelting is adhesive wear, abrasive wear, and delamination wear. The wear characteristics of the worn surface are consistent with the analysis results obtained from Fig.7 and Fig.8. Fig.9b and 9e show the morphologies of wear debris from the FeCrMnAlCu HEA coating synthesized by cold spraying-assisted induction remelting and laser remelting, respectively. Not only the two wear debris, but also their particles are similar. Fig.9c and 9f show XRD patterns of wear debris in FeCrMnAlCu HEA coating synthesized by cold spraying-assisted induction remelting and laser remelting, respectively. The main components of the wear debris of these two coatings are the bcc phase and fcc phase. A small amount

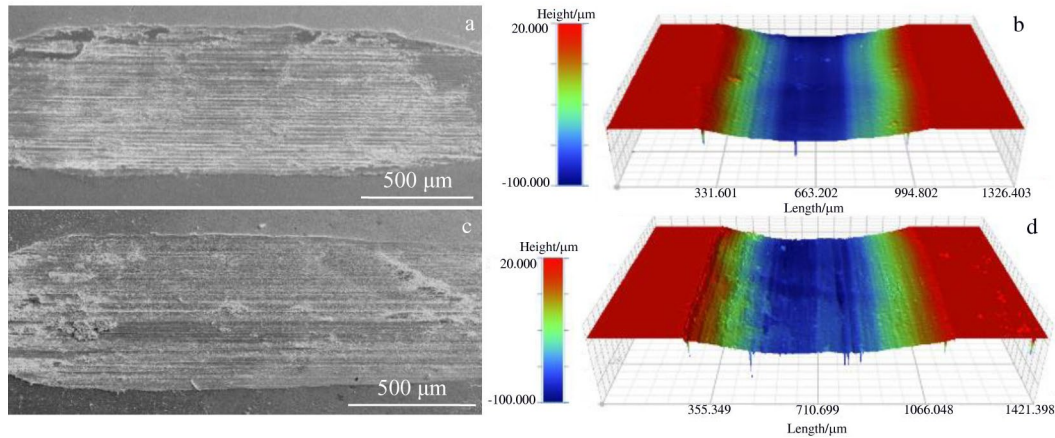


Fig.8 Friction and wear morphologies (a, c) and corresponding 3D wear morphologies (b, d) of FeCrMnAlCu HEA coatings prepared by cold spraying-assisted induction remelting (a, b) and laser remelting (c, d)

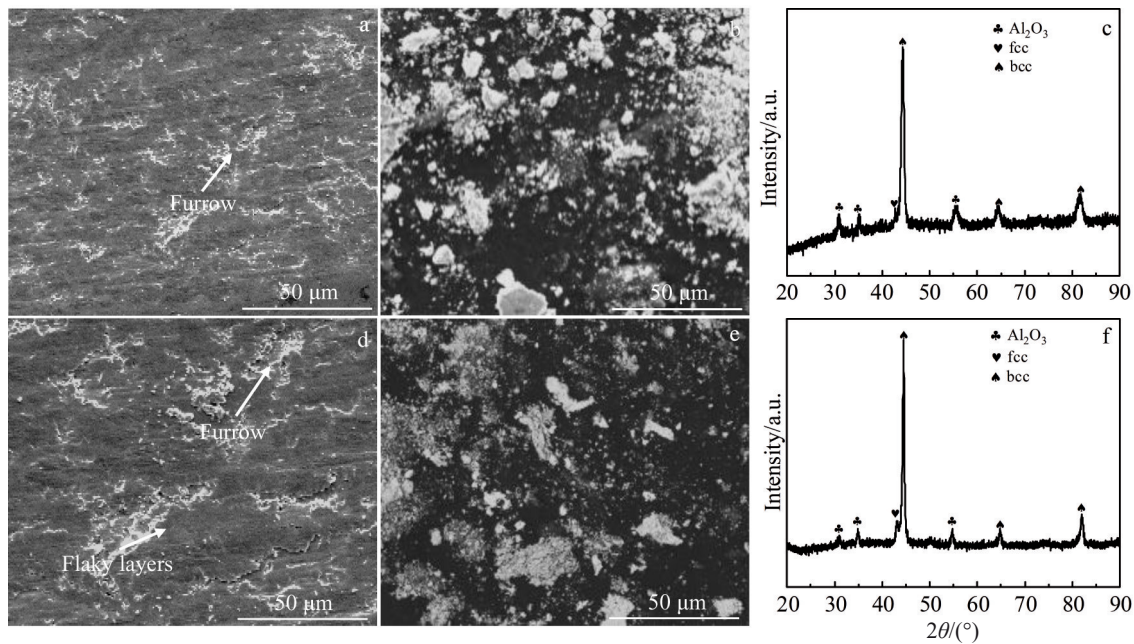


Fig.9 Morphologies of wear surfaces (a, d) and wear debris (b, e) and XRD patterns of wear debris (c, f) of FeCrMnAlCu HEA coatings prepared by cold spraying-assisted induction remelting (a–c) and laser remelting (d–f)

of Al_2O_3 is detected in both wear debris, and no other oxides are detected in the wear debris. This result indicates that the Al_2O_3 originates from the friction pair and no oxidation reaction occurs in the friction process.

3 Conclusions

1) The FeCrMnAlCu high-entropy alloy (HEA) coating synthesized by cold spraying-assisted induction remelting and laser remelting are mainly composed of dendrite with rich Mn, Cr, and Fe and the interdendrite with rich Cu element. In addition, Al element is evenly distributed between the dendrite and interdendrite regions. The laser remelting process has concentrated energy and high temperature, resulting in the thick heat-affected zone and Fe diffusion into the coating. Thus, more Fe appears between dendrite and interdendrite regions.

2) The microstructure of FeCrMnAlCu HEA coating synthesized by cold spraying-assisted induction remelting and laser remelting is composed of body-centered cubic (bcc) dendrite and face-centered cubic (fcc) interdendrite. The Fe content in FeCrMnAlCu HEA coating synthesized by cold spraying-assisted laser remelting is relatively high, which leads to the lattice distortion of bcc and fcc structures. The change in lattice constant of FeCrMnAlCu HEA coating synthesized by cold spraying-assisted laser remelting is less than that synthesized by cold spraying-assisted induction remelting.

3) The microhardness of the FeCrMnAlCu HEA coating synthesized by cold spraying-assisted induction remelting is 5742.8 MPa, which is 1.2 times higher than that synthesized by cold spraying-assisted laser remelting, and 3.5 times higher

than that of 45# steel matrix. This is because the proportion of bcc dendrite structure in HEA coating prepared by cold spraying-assisted induction remelting is larger than that prepared by cold spraying-assisted laser remelting. In addition, the lattice strains of the bcc and fcc structures in HEA coating prepared by cold spraying-assisted induction remelting are larger than those in HEA coating prepared by cold spraying-assisted laser remelting.

4) The friction coefficients of FeCrMnAlCu HEA coatings synthesized by cold spraying-assisted induction remelting and laser remelting are 0.35 and 0.48, respectively, and the wear rates are 2.95×10^{-5} and $4.14 \times 10^{-5} \text{ mm}^3 \cdot \text{N}^{-1} \cdot \text{m}^{-1}$, respectively. The FeCrMnAlCu HEA coating synthesized by cold spraying-assisted induction remelting has better wear resistance.

References

- 1 Yeh J W, Chen S K, Lin S J et al. *Advanced Engineering Materials*[J], 2004, 6(5): 299
- 2 Cantor B, Chang I T H, Knight P et al. *Materials Science and Engineering A*[J], 2004, 375-377: 213
- 3 Kai W, Cheng F P, Liao C Y et al. *Materials Chemistry and Physics*[J], 2018, 210: 362
- 4 Tsai M H, Yeh J W. *Materials Research Letters*[J], 2014, 2(3): 107
- 5 Miracle D B, Senkov O N. *Acta Materialia*[J], 2017, 122: 448
- 6 Yeh J W. *JOM*[J], 2013, 65(12): 1759
- 7 Zhou Y J, Zhang Y, Wang Y L et al. *Materials Science and Engineering A*[J], 2007, 454: 260
- 8 Qiu Y, Thomas S, Gibson M A et al. *npj Materials Degradation*[J], 2017, 1(1): 15
- 9 Chuang M H, Tsai M H, Wang W R et al. *Acta Materialia*[J], 2011, 59(16): 6308
- 10 Fu Z Q, Jiang L, Wardini J L et al. *Science Advances*[J], 2018, 4(10): eaat8712
- 11 Li Y Z, Shi Y. *Optics and Laser Technology*[J], 2021, 134: 106 632
- 12 Qiu X W, Zhang Y P, He L et al. *Journal of Alloys and Compounds*[J], 2013, 549: 195
- 13 Chen L, Bobzin K, Zhou Z et al. *Surface and Coatings Technology*[J], 2019, 358: 215
- 14 Ge W J, Wu B, Wang S R et al. *Advanced Powder Technology*[J], 2017, 28(10): 2556
- 15 Raman L, Anupam A, Karthick G et al. *Materials Science and Engineering A*[J], 2021, 819: 141 503
- 16 Totten G E, Xie L, Funatani K. *Handbook of Mechanical Alloy Design*[M]. New York: Marcel Dekker, 2004
- 17 Ye Q F, Feng K, Li Z G et al. *Applied Surface Science*[J], 2017, 396: 1420
- 18 Wong S K, Shun T T, Chang C H et al. *Materials Chemistry and Physics*[J], 2018, 210: 146
- 19 Liao W B, Wu Z X, Lu W et al. *Intermetallics*[J], 2021, 132: 107 138
- 20 Yin S, Li W Y, Song B et al. *Journal of Materials Science and Technology*[J], 2019, 35(6): 1003
- 21 Feng Li, Wang Jun, Wang Guiping et al. *Rare Metal Materials and Engineering*[J], 2021, 50(11): 3987 (in Chinese)
- 22 Han C, Ma L, Sui X D et al. *Coatings*[J], 2021, 11(6): 695
- 23 Wang Y, Lu X X, Yuan N Y et al. *Journal of Alloys and Compounds*[J], 2020, 849: 156 222
- 24 Zhang Y, Zuo T T, Tang Z et al. *Progress in Materials Science*[J], 2014, 61: 1
- 25 Yang X, Zhang Y. *Materials Chemistry and Physics*[J], 2012, 132(2-3): 233
- 26 Guo S, Hu Q, Ng C et al. *Intermetallics*[J], 2013, 41: 96
- 27 Praveen S, Murty B S, Kottada R S. *Materials Science and Engineering A*[J], 2012, 534: 83
- 28 Qiu X W. *Journal of Alloys and Compounds*[J], 2018, 735: 359
- 29 Feng L, Yang W J, Ma K et al. *Materials Technology*[J], 2022, 37(13): 2567

感应重熔和激光重熔合成 FeCrMnAlCu 高熵合金涂层组织与性能

马 凯¹, 冯 力^{1,2}

(1. 兰州理工大学 材料科学与工程学院, 甘肃 兰州 730050)

(2. 兰州理工大学 省部共建有色金属先进加工与再利用国家重点实验室, 甘肃 兰州 730050)

摘要: 采用冷喷涂辅助感应重熔和冷喷涂辅助激光重熔2种方法分别在45#钢表面制备FeCrMnAlCu高熵合金涂层。对高熵合金涂层的相组成、显微组织、硬度、耐磨性能进行表征与检测, 研究2种工艺对涂层耐磨性能的影响。结果表明: 2种工艺合成的FeCrMnAlCu高熵合金涂层均由体心立方(bcc)和面心立方(fcc)相组成, 涂层组织致密, 元素分布均匀。涂层微观组织均为树枝晶+枝晶间组织, 枝晶区主要由Mn、Cr和Fe元素构成, 枝晶间主要为Cu, Al元素均匀地分布在枝晶和枝晶间。冷喷涂辅助感应重熔合成的FeCrMnAlCu高熵合金涂层中bcc晶格应变大于激光重熔合成的高熵合金涂层的晶格应变。冷喷涂辅助感应重熔合成FeCrMnAlCu高熵合金涂层的显微硬度是冷喷涂辅助激光重熔合成涂层硬度的1.2倍, 是45#钢基体硬度的3.5倍。FeCrMnAlCu高熵合金涂层在摩擦过程中主要以磨粒磨损为主, 采用冷喷涂辅助感应重熔合成的FeCrMnAlCu高熵合金涂层具有良好的耐磨性能, 其磨损率比冷喷涂辅助激光重熔合成涂层的磨损率降低29%。

关键词: 感应重熔; 激光重熔; 高熵合金涂层; 晶格应变

作者简介: 马 凯, 男, 1995年生, 博士生, 兰州理工大学材料科学与工程学院, 甘肃 兰州 730050, E-mail: mkysys131477@163.com